

Interannual modulation of eddy kinetic energy in the southeast Indian Ocean by Southern Annular Mode

Fan Jia,¹ Lixin Wu,¹ Jian Lan,¹ and Bo Qiu²

Received 2 October 2010; revised 19 November 2010; accepted 8 December 2010; published 19 February 2011.

[1] Interannual variability in the mesoscale eddy field over the southeast Indian Ocean of 15°S–35°S and 60°E–110°E is investigated on the basis of 16 year satellite altimetry observations. Eddy kinetic energy (EKE) in this region appears stronger in 2000–2004 and weaker in 1993–1996, 1998–2000, and 2007. It is found that this interannual modulation of EKE is mediated by the Southern Annular Mode (SAM), with a positive (negative) SAM corresponding to weak (strong) eddy activity in this region. The interannual modulation of the EKE by the SAM is through modulating the baroclinic instability associated with the surface-intensified South Indian Countercurrent (SICC) and the underlying South Equator Current (SEC) system. In the positive phase of the SAM, the southeastern subtropical Indian Ocean is dominated by an anomalous Ekman upwelling, which slackens the southward tilt of the isotherms and thus reduces the SICC. This shall reduce the vertical velocity shear of the SICC-SEC current system, leading to a weak instability and thus a weak eddy activity.

Citation: Jia, F., L. Wu, J. Lan, and B. Qiu (2011), Interannual modulation of eddy kinetic energy in the southeast Indian Ocean by Southern Annular Mode, *J. Geophys. Res.*, 116, C02029, doi:10.1029/2010JC006699.

1. Introduction

[2] Ocean mesoscale eddies play an important role in determining large-scale ocean circulations and transport of momentum, heat, freshwater and nutrients. Recent studies of satellite altimeter observations have provided evidence that the large-scale climatic variations, for instance, the Pacific Decadal Oscillation (PDO) [e.g., Qiu and Chen, 2010b] and the North Atlantic Oscillation (NAO) [e.g., Eden and Böning, 2002; Penduff et al., 2004] can modulate eddy activities over the extratropical North Pacific and Atlantic, respectively.

[3] Vigorous eddy activities have been found in the western boundary current regions because of their strong nonlinearity. High eddy kinetic energy (EKE) has been also detected in the southeast Indian Ocean (15°S–35°S, 60°E–110°E) [Jia et al., 2011]. This high-EKE band is located in the region of the South Indian Ocean Countercurrent (SICC) [Siedler et al., 2006; Palastanga et al., 2007]. The eastward flowing SICC extends above the deep reaching, westward flowing SEC, forming a unique baroclinic current system similar to the STCC-NEC system in the North Pacific [Qiu, 1999; Qiu and Chen, 2010a]. The EKE over the southeast Indian Ocean displays a distinct seasonal cycle, which has been demonstrated to be associated with the baroclinic instability of the SICC-SEC system because of seasonal

changes of the wind-induced Ekman convergence and surface heat flux [Jia et al., 2011].

[4] While the seasonal variability of the EKE over the southeast Indian Ocean is predominantly by local forcing, it is naturally wondered whether there are significant variations at interannual time scales. This question is raised because the southeast Indian Ocean is subject to multiple forcing of large-scale climate variations including the Indian Ocean dipole event [Saji et al., 1999; Webster et al., 1999], the Indian Ocean basin mode [Yang et al., 2007], the El Niño–Southern Oscillation (ENSO), and the Southern Annular Mode (SAM) [Thompson and Wallace, 2000] (see a recent review by Schott et al. [2009]).

[5] On the basis of the 16 year satellite altimetry observations, here we found that the EKE in the southeast Indian Ocean indeed displays significant interannual variability, which is mainly mediated by the SAM. The SAM is the dominant mode of atmospheric variability in the Southern Hemisphere [Thompson and Wallace, 2000; Marshall, 2003]. Studies have indicated that the SAM cannot only influence climate in the Antarctic regions but also the subtropical oceans [Thompson and Wallace, 2000; Mo, 2000; Hall and Visbeck, 2002; Marshall et al., 2006; Silvestri and Vera, 2009]. In particular, Hall and Visbeck [2002] found that in the atmosphere, the positive SAM is associated with an intensification of the westerlies at about 55°S and a weakening at about 35°S, which accounts for nearly all the variability in zonal-mean surface winds at these locations. In addition, the meridional poleward heat transport for a positive SAM is increased by about 15% around 30°S and reduced by ~20% in the circumpolar region. A more recent modeling study by Ma and Wu [2011] suggests that the oceanic changes in the ACC region can impact the southeast trades more

¹Physical Oceanography Laboratory, Ocean University of China, Qingdao, China.

²Department of Oceanography, University of Hawai'i at Mānoa, Honolulu, Hawaii, USA.

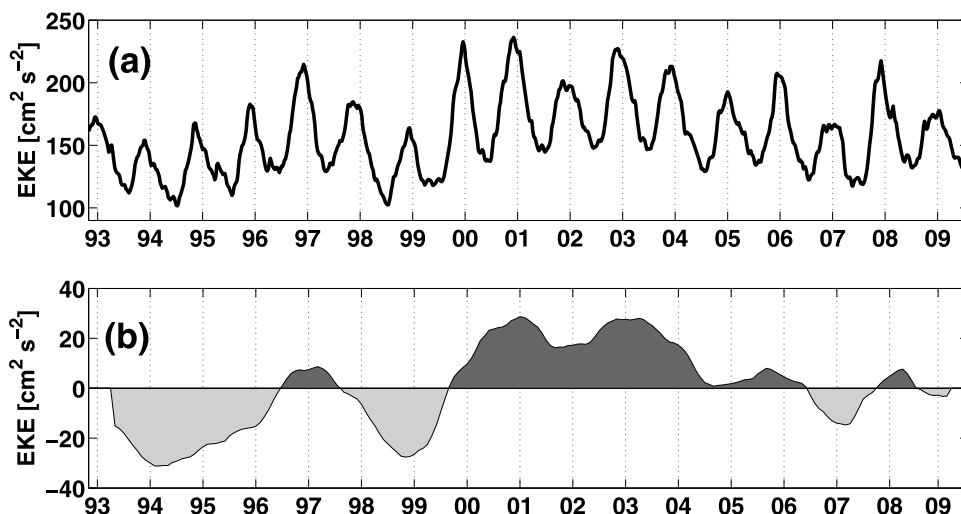


Figure 1. (a) Time series of EKE averaged in the southeast Indian Ocean (15°S–35°S, 60°E–110°E). (b) One year low-pass-filtered EKE in Figure 1a.

effectively through the surface wind–evaporation–SST (WES) coupled feedback at seasonal time scales. In this study, we found that the EKE in the southeast Indian Ocean can be modulated substantially by the SAM.

[6] The paper is outlined as follows. In section 2, we start with a brief description of the data used here. The interannual variability of EKE in the southeast Indian Ocean is presented in section 3. Section 4 discusses the influence of different large-scale climate variability modes. Section 5 explores the mechanism underlying the interannual EKE variability through stability analysis. The paper is concluded with a summary and discussions in section 6.

2. Data

[7] The data used in this study, including temperature, currents, surface wind stresses and net surface heat flux, are all from the ocean reanalysis product Simple Ocean Data Assimilation (SODA 2.0.2–4) [Carton *et al.*, 2000]. The SODA product is available in the monthly average format with a grid of $0.5^\circ \times 0.5^\circ \times 40$ level. The SODA has a climatology similar to observations (not shown), and been used in the past to study the Indian Ocean interannual climate variability, for example, by Xie *et al.* [2002] and Rao and Behera [2005].

[8] We also use the satellite altimetry “Ref” (M) SLA Delayed Time Products produced by Ssalto/Duacs and distributed by Aviso with support from the CNES, which contain the multimission (T/P, ERS-1/2, Jason-1, Jason-2) gridded sea surface heights computed with respect to a 7 year mean. The data set has a weekly format on a $1/3^\circ \times 1/3^\circ$ Mercator grid and covers the period from October 1992 to July 2009.

[9] For the climate indices in section 4, the Nino3.4 index is directly taken from the Earth System Research Laboratory of NOAA (<http://www.esrl.noaa.gov/psd/forecasts/sstlim/timeseries/>), and the SAM index is taken from the Climate Prediction Center (CPC) (http://www.cpc.noaa.gov/products/precip/CWlink/daily_ao_index/aao/aao.shtml). The loading pattern of SAM is defined as the first leading mode from the

EOF analysis of monthly mean 700 hPa height anomalies poleward of 20° latitude for the Southern Hemisphere. Monthly SAM indices are constructed by projecting the monthly mean 700 hPa height anomalies onto the leading EOF mode and then normalized by the standard deviation of the monthly index (1979–2000 base period). The IOB index is calculated as the SST anomaly averaged in the tropical Indian Ocean (20°S – 20°N , 40°E – 120°E). Following Saji *et al.* [1999], the IOD index is defined as the difference in SST anomaly between the tropical western Indian Ocean (50°E – 70°E , 10°S – 10°N) and the tropical southeastern Indian Ocean (90°E – 110°E , 10°S –equator). The SST data using here is from the Hadley Center Sea Surface Temperature data set (HadISST) [Rayner *et al.*, 2003].

3. Interannual Changes of EKE in the Southeast Indian Ocean

[10] The EKE is estimated on the basis of geostrophic calculation as follows:

$$EKE = \frac{1}{2} [U_g'^2 + V_g'^2] \quad (1)$$

$$U_g' = -\frac{g}{f} \frac{\Delta\eta'}{\Delta y}, V_g' = \frac{g}{f} \frac{\Delta\eta'}{\Delta x}$$

where U_g' and V_g' are the geostrophic velocities, f the Coriolis parameter, and η' the SLA.

[11] Figure 1a shows the time series of EKE averaged in the southeast Indian Ocean (15°S – 35°S , 60°E – 110°E). Notice that EKE in this region displays a distinct seasonal cycle with maximum in austral summer (November–December–January) and minimum in austral winter (May–June–July). In addition to the seasonal variation, the EKE in the southeast Indian Ocean also displays significant interannual variability with weak eddy activities in 1993–1996, 1998–2000, 2007, strong eddy activities in 2000–2004, and normal eddy activities in 1995, 2005–2006, and 2008–2009 (Figure 1b). The spatial pattern of the EKE between eddy-rich and eddy-weak years is demonstrated in Figure 2. An

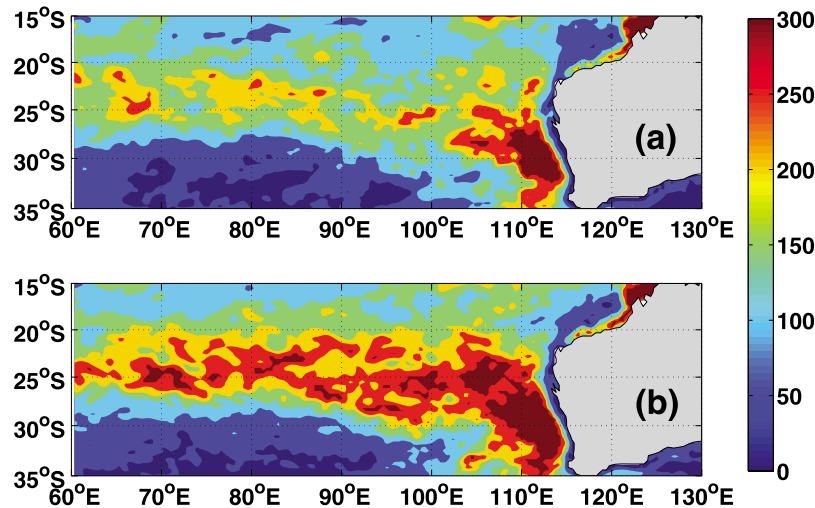


Figure 2. Composite EKE in the southeast Indian Ocean for (a) eddy-weak years (1993–1996 and 1998–2000) and (b) eddy-rich years (2000–2004).

intensification of eddy activity is clearly identified in the region (60°E – 110°E , 20°S – 30°S) in 2000–2004. The peak-to-peak amplitude of the EKE interannual variability is about 50 – $60\text{ cm}^2/\text{s}^2$, which accounts for about 40% of the regional mean EKE level (Figure 1b).

[12] The EKE also displays a pronounced westward propagation, with propagation speed determined by Rossby waves (Figure 3). The strongest signals occur east of 90°E , with amplitude decaying toward west. This suggests that the east of 90°E could be the important source for eddy genesis.

4. Correlation Between EKE and Large-Scale Climate Variability Modes

[13] The interannual variability of the eddy activities in the southeastern Indian Ocean may be influenced by different large-scale climate variability modes including ENSO, Indian Ocean basin mode (IOB), Indian Ocean dipole mode (IOD) and the SAM. In order to clarify the dominant factors, we compare the EKE time series and indices of these different modes (Figure 4). As shown in Figure 4, all these modes display significant interannual variability. Among these large-scale variability modes, the SAM exhibits the strongest phase coherence with the EKE in the southeastern Indian Ocean (Figure 4g). The maximum correlation reaches -0.3 (significant at 95% significance level) when the SAM leads the EKE by about 4 months (Figure 4h). For example, a positive SAM in 1993–1996 and 1998–1999 corresponds to weak eddy activity, while a negative SAM in 2000–2004 corresponds to strong eddy activity. In the following, we will focus on the influence of the SAM on the EKE in the southeast Indian Ocean.

5. Formation Mechanism of EKE Interannual Variability

5.1. Stability Analysis

[14] In our early study, it is found that the seasonal variation of the EKE in this region is associated with baroclinic instability of the SICC–SEC current system [Jia *et al.*,

2011]. By following that, here we first examine how the background circulation of the SICC–SEC system changes in the weak and strong eddy activity years.

[15] Figure 5 shows the mean flow field derived from SODA data during the eddy-weak and eddy-rich years. We focus on the subdomain (15°S – 35°S , 100°E – 110°E) rather than the entire zonal band because this region is the source of mesoscale eddy activities. As shown in Figure 5, the SEC extends from 10°S to 40°S and reaches 500 m depth. In contrast, the eastward flowing SICC is weaker and shallow, with its core located at 20°S – 30°S and trapped in the upper 200 m. In the eddy-rich years, the westward flowing SEC appears to be not significantly different from that in the

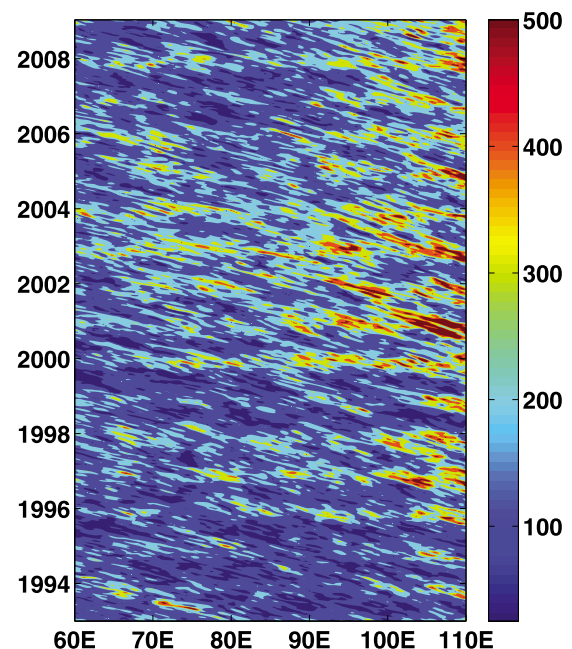


Figure 3. Time-longitude plot of EKE along 20°S – 30°S in the southeast Indian Ocean from January 1993 to December 2008.

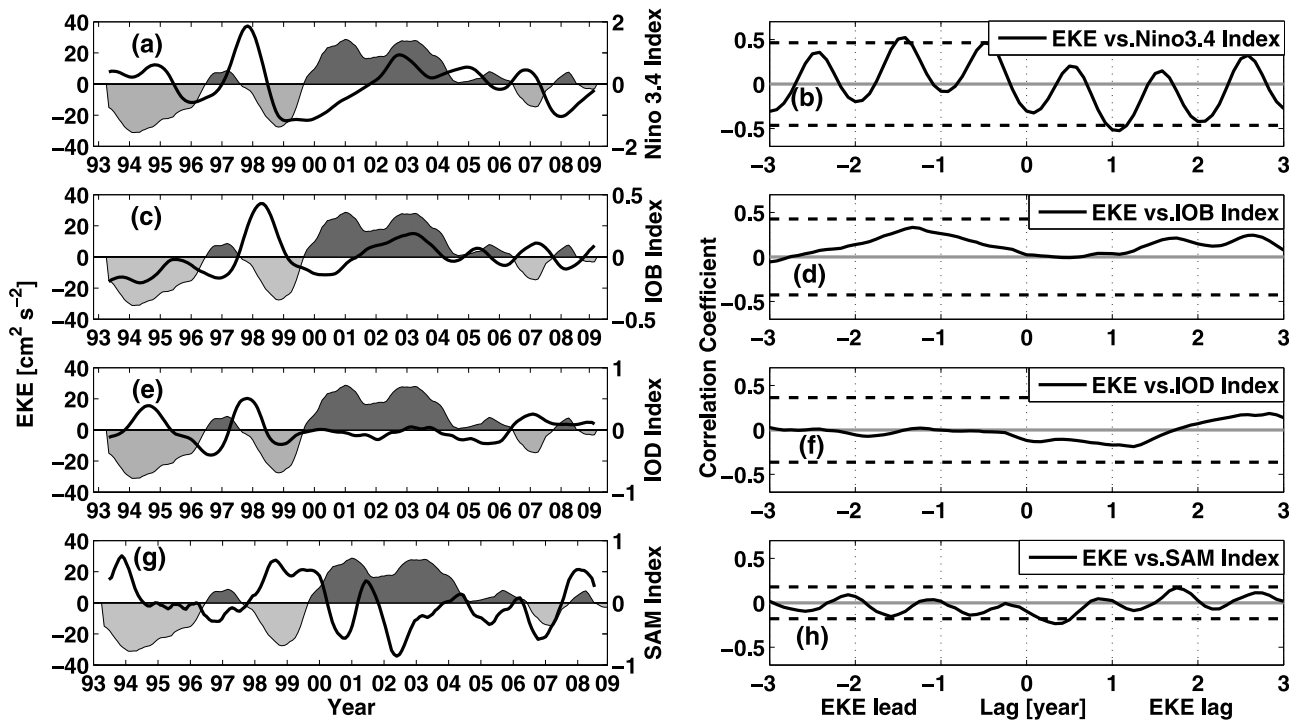


Figure 4. Time series and correlation of the EKE in the southeast Indian Ocean and different climate variability mode indices: (a, b) Nino3.4 index, (c, d) IOB index, (e, f) IOD index, and (g, h) SAM index. All indices are low-pass filtered (>1 year), and the dashed lines indicate 95% significance level.

weak-eddy years, but the eastward flowing SICC appears to be stronger than that in the weak-eddy years. The changes in the velocity become clearer in Figure 6 where the vertical profile of the zonal velocity is shown. The change of the SICC reaches about 0.7 cm/s, accounting for about 50% of the mean speed; while the change of the SEC is about 0.1 cm/s, which only accounts for about 10% of the mean speed. Here we define the vertical velocity shear as the zonal velocity difference between the upper (50 m) and lower (300 m) layers. So, the vertical velocity shear is

stronger in the eddy-rich years (~0.033 m/s) than in the eddy-weak years (~0.027 m/s).

[16] In order to clarify how the interannual variation of EKE relates to the vertical shear, both of them are displayed in Figure 7. The variations of the vertical velocity shear correlate well with the EKE with a lead of a few months (Figure 7a). This is confirmed in Figure 7b, which shows that the maximum correlation between the two time series occurs when the vertical shear leads the EKE by ~5 months.

[17] How does the change of the vertical shear associated with the SICC-SEC current system modify the EKE level?

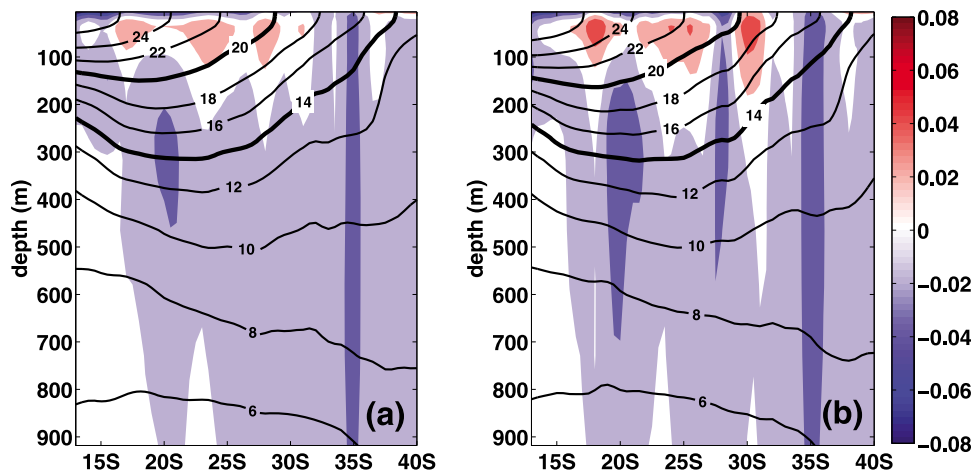


Figure 5. Latitude-depth profile of temperature (solid contours, units °C) and zonal velocity (shading, units $m s^{-1}$) along 100°E–110°E in the southeast Indian Ocean during (a) eddy-weak years and (b) eddy-rich years.

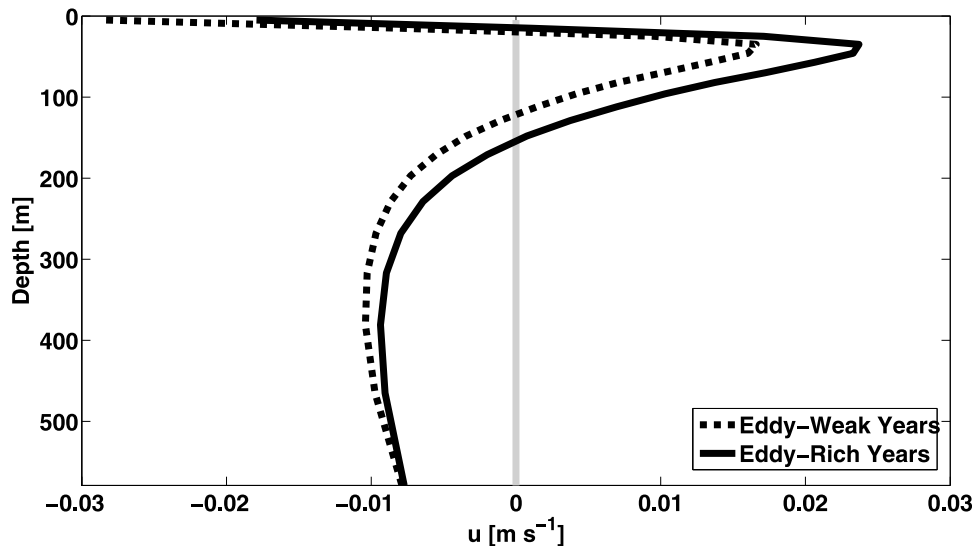


Figure 6. Vertical profiles of zonal velocity averaged over the region (15°S–35°S, 100°E–110°E) in eddy-weak (dotted line) and eddy-rich (solid line) years.

Following *Qiu* [1999], we adopt a 2.5-layer reduced-gravity model with two active upper layers and an infinitely deep abyssal layer to analyze the stability of the SICC-SEC current system. This method was also used in analyzing the seasonal modulation of EKE in this region [*Jia et al.*, 2011]. The governing quasi-geostrophic equation for the active two upper layers can be expressed by

$$\left(\frac{\partial}{\partial t} + U_n \frac{\partial}{\partial x}\right) q_n + \frac{\partial \Pi_n}{\partial y} \frac{\partial \phi_n}{\partial x} = 0 \quad (2)$$

where U_n is the zonal geostrophic velocity, q_n the perturbation potential vorticity, ϕ_n the perturbation stream function, Π_n the mean potential vorticity in the n th layer ($n = 1$

and 2). Assume that the mean flow U_n is meridionally uniform, q_n and the meridional gradient of Π_n can be expressed by

$$q_n = \nabla^2 \phi_n + \frac{(-1)^n}{\lambda_n^2} (\phi_1 - \phi_2 - \gamma_n \phi_2) \quad (3)$$

$$\Pi_{ny} = \beta - \frac{(-1)^n}{\lambda_n^2} (U_1 - U_2 - \gamma_n U_2) \quad (4)$$

where $\gamma_n = \frac{\rho_n - \rho_1}{\rho_3 - \rho_2}$ is the stratification ratio, $\lambda_n^2 = \frac{(\rho_2 - \rho_1)gH_n}{\rho_0 f_0^2}$ is the square of the internal Rossby radius in layer n , $\beta = \frac{2\Omega \cos \phi_0}{R}$ and f_0 is the Coriolis parameter at the reference latitude 25°S.

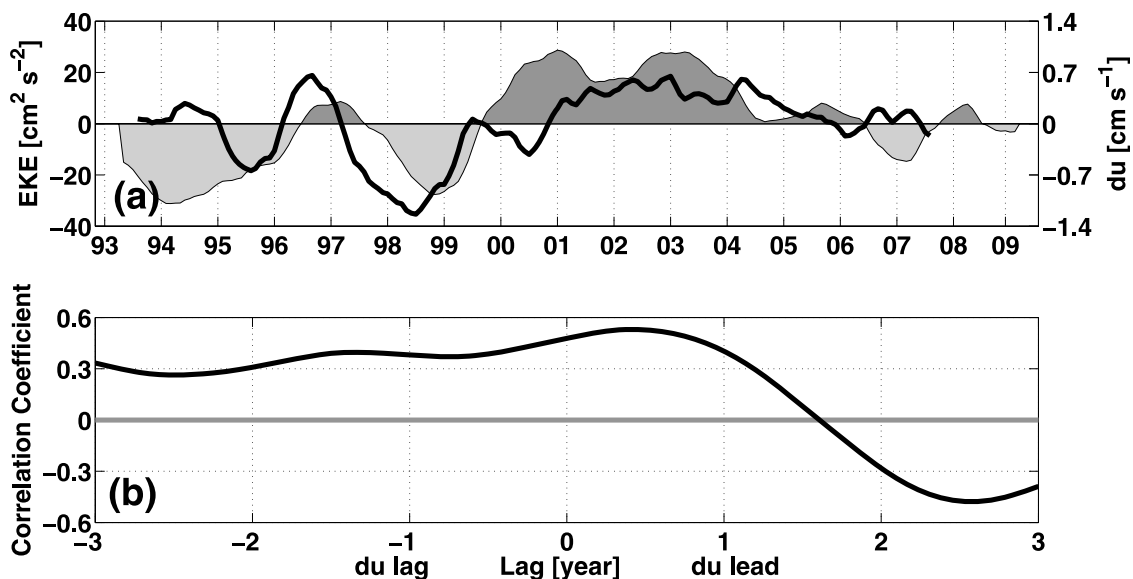


Figure 7. (a) EKE (shaded areas) and vertical velocity shear (solid line). (b) Lagged correlation between EKE and vertical velocity shear shown in Figure 7a. The vertical velocity shear is defined as $du = u(50 \text{ m}) - u(300 \text{ m})$ using the SODA product averaged in (15°S–35°S, 100°E–110°E). All time series are smoothed by applying a 1 year low-pass filter.

Table 1. Parameter Values of the Region 15°S–35°S, 100°E–110°E in Eddy-Weak and Eddy-Rich Years^a

Parameter	Eddy-Weak Years	Eddy-Rich Years
f_0	$-6.16 \times 10^{-5} \text{ s}^{-1}$	$-6.16 \times 10^{-5} \text{ s}^{-1}$
β	$2.07 \times 10^{-11} \text{ s}^{-1} \text{ m}^{-1}$	$2.07 \times 10^{-11} \text{ s}^{-1} \text{ m}^{-1}$
U_1	0.0174 m s^{-1}	0.0229 m s^{-1}
U_2	-0.01 m s^{-1}	-0.01 m s^{-1}
H1	150 m	150 m
H2	300 m	300 m
ρ_1	$24.40 \sigma_\theta$	$24.40 \sigma_\theta$
ρ_2	$26.71 \sigma_\theta$	$26.71 \sigma_\theta$
ρ_3	$27.80 \sigma_\theta$	$27.80 \sigma_\theta$

^aThe reference latitude for f_0 and β is taken at 25°S; the other parameter values are estimated from the SODA data.

[18] Assume that equation (2) has a normal mode solution:

$$\phi_n = A_n \cos(kx + ly - kct) \quad (5)$$

substituting ϕ_n into equation (2) and a dispersion relationship as well as the necessary and sufficient condition for instability in the 2.5-layer model can be obtained:

$$c^2 - \left(U_1 + U_2 - \frac{P+Q}{R} \right) c + \left(U_1 U_2 + \frac{\Pi_{1y} \Pi_{2y}}{R} - \frac{U_1 P}{R} - \frac{U_2 Q}{R} \right) = 0 \quad (6)$$

and

$$(U_1 - U_2)_{\min} > \lambda_2^2 \beta + \gamma_2 U_2 \quad (7)$$

where P , Q and R are functions of k , l , δ and λ (see *Qiu* [1999] and *Qiu and Chen* [2004] for details). Equation (6) is the dispersion relationship for the complex wave speed c ($c = c_r + ic_i$) from which we may detect the growth rate (kc_i) of the SICC-SEC system and compare with the observed results. The instability criterion equation (7) implies that once the condition (7) is satisfied, the system becomes baroclinically unstable. With the parameters appropriate for the southeast Indian Ocean (Table 1), this

requires $U_1 > \lambda_2^2 \beta + (\gamma_2 + 1) U_{2\max} = -0.08 \text{ cm s}^{-1}$. In the SICC-SEC system, the eastward flow SICC never changes directions, so the system is always baroclinic unstable.

[19] With the parameters in Table 1, the dispersion relationship (equation (6)) is solved and the growth rates for the unstable waves are displayed in Figure 8. The system is unstable under both eddy-weak and eddy-rich conditions ($c_i \neq 0$) and the preferred wavelength scale of the most unstable waves is $\sim 200 \text{ km}$, which corresponds well with the observed mesoscale eddy propagation wavelength scale. But there are also many differences. The most unstable wave in eddy-rich years has $kc_i = 0.01 \text{ d}^{-1}$, or an e -folding time scale of 100 days (Figure 8b), while the most unstable wave in eddy-rich years is 0.007 d^{-1} or an e -folding time scale of 140 days (Figure 8a). In addition, the window for permissible unstable waves in eddy-rich years is broader than that in eddy-weak years (Figure 8b versus Figure 8a). Therefore, the system in eddy-rich years is baroclinically more unstable than that in eddy-weak years.

[20] Notice that the major difference between the two is the parameter U_1 or the vertical velocity shear. In eddy-rich years U_1 is 0.0229 m s^{-1} and the vertical shear $U_1 - U_2$ is 0.033 m s^{-1} ; well in eddy-weak years U_1 decreases to 0.0174 m s^{-1} and $U_1 - U_2$ is 0.027 m s^{-1} . The stronger vertical velocity shear in eddy-rich years work to intensify baroclinic instability and result in enhanced mesoscale eddy activities after the e -folding time scale of the unstable waves.

[21] In summary, the 2.5-layer reduced-gravity model results support the argument that the interannual variation in the intensity of baroclinic instability of the SEC-SICC current system caused by the vertical shear modulates the eddy kinetic energy in the southeast Indian Ocean.

5.2. Modulation of the Vertical Velocity Shear by SAM

[22] According to the analysis above, the vertical velocity shear plays an important role in modulating the interannual changes of EKE in the southeast Indian Ocean. In the following, we will analyze how the SAM modulates the vertical velocity shear. The vertical velocity shear can be

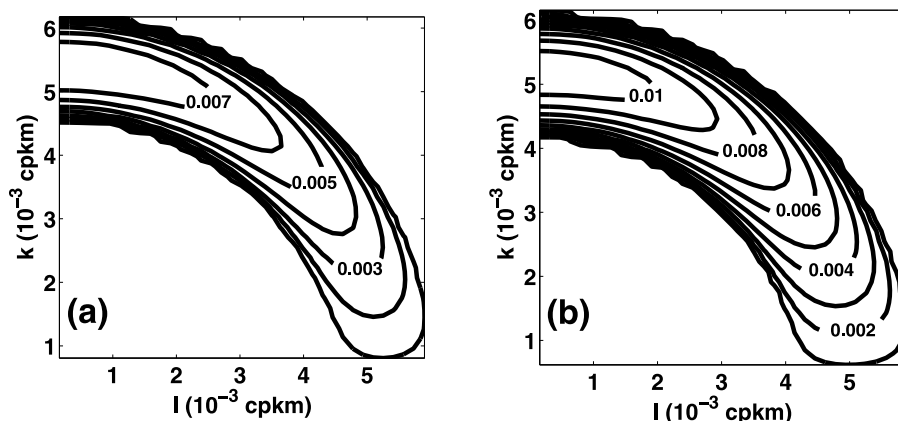


Figure 8. Growth rate of unstable waves as a function of zonal and meridional wave number for (a) eddy-weak years and (b) eddy-rich years. Units for the growth rate are d^{-1} . Parameters used in the analysis are averaged in (15°S–35°S, 100°E–110°E).

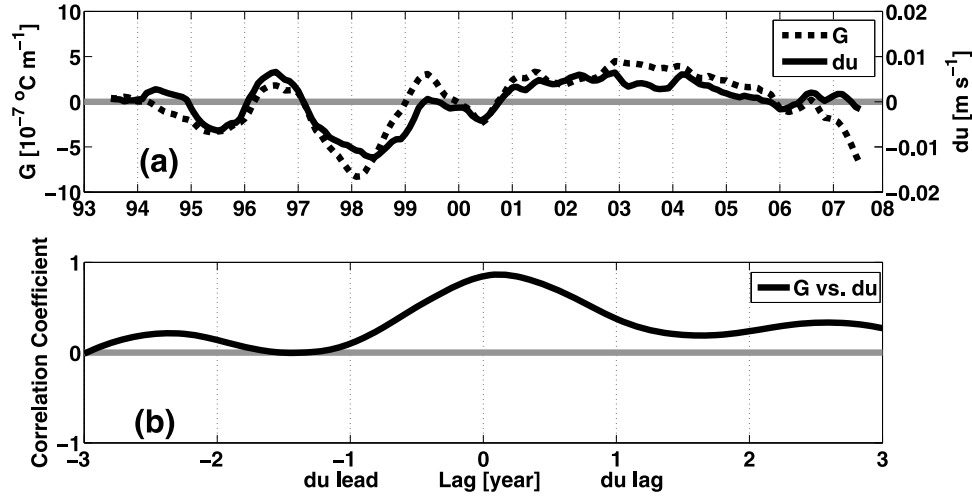


Figure 9. (a) G (dotted line) and vertical velocity shear (solid line). (b) Lagged correlation between G and vertical velocity shear shown in Figure 9a. Both time series are smoothed by applying a 1 year low-pass filter. G is averaged in (15°S–35°S, 100°E–110°E) over upper 150 m.

related to the meridional temperature gradient through the thermal wind balance:

$$f \frac{\partial U_g}{\partial z} = -\alpha g \frac{\partial T}{\partial y} \quad (8)$$

where f is the Coriolis parameter and α the thermal expansion coefficient. We define $G \equiv \partial T / \partial y$ and a positive G indicates an enhanced isotherm slope and thus vertical shear. Here we ignore salinity in equation (8) since the salinity effect is of secondary importance [Jia *et al.*, 2011]. This can also be proved by Figure 9: the interannually changed G (dotted line) and the vertical velocity shear (solid line) behave quite similarly with a synchronous correlation coefficient ~ 0.9 .

[23] From the governing equation for temperature, we have

$$\begin{aligned} \frac{\partial G}{\partial t} &= \frac{\partial}{\partial y} \left(\frac{\partial T}{\partial t} \right) = \frac{\partial}{\partial y} \left(-v \frac{\partial T}{\partial y} - w \frac{\partial T}{\partial z} + \frac{Q_{net}}{\rho_o C_p H_1} + diff \right) \\ &= -\frac{\partial}{\partial y} [(v_g + v_{Ek})G] - \frac{\partial}{\partial z} (wG) + \frac{\partial}{\partial y} \left(\frac{Q_{net}}{\rho_o C_p H_1} \right) + \frac{\partial}{\partial y} (diff) \end{aligned} \quad (9)$$

where $v_{Ek} = -\tau^x / \rho_o f H_0$ is the meridional Ekman velocity averaged in the surface layer, τ^x the zonal wind stress, ρ_o the reference density, Q_{net} net surface heat flux, C_p the specific heat of ocean water, $diff$ the diffusion terms, u_g/v_g the zonal/meridional geostrophic velocity, u_{Ek}/v_{Ek} the zonal/meridional Ekman velocity and H_1 the thickness of the surface layer. Here, H_1 is set to 150 m. In equation (9), we have neglected the zonal temperature gradient advection term because only the zonally averaged G is concerned here. On the basis of the SODA product, the vertical advection and diffusion ($-\frac{\partial}{\partial z}(wG) + \frac{\partial}{\partial y}(diff)$) can be also neglected. With this, equation (9) can be further simplified to

$$\frac{\partial G}{\partial t} \approx -\frac{\partial}{\partial y} (v_{Ek}G) - \frac{\partial}{\partial y} (v_g G) + \frac{\partial}{\partial y} \left(\frac{Q_{net}}{\rho_o C_p H_1} \right) \quad (10)$$

[24] Physically, it indicates that changes in G are largely controlled by the combined forcings: the meridional Ekman forcing, the meridional geostrophic forcing and the meridional surface heat flux forcings. Interannual changes in the each forcing and the combined forcings derived from the SODA product as well as the SAM index are shown in Figure 10. It can be seen that the meridional geostrophic forcing plays a dominant role, while the meridional Ekman forcing and surface heat flux forcings are less important. The combined forcing is negatively correlated with the SAM: a positive SAM corresponds to a weak forcing (Figure 10b) and thus weak vertical shear (Figure 10b) (the phase delay is expected because of the time derivative in the forcing) and eddy activity, and vice versa.

[25] How does the SAM affect the forcing of the meridional temperature gradient? Physically it can be understood as follow. As shown in Figure 11a, a positive SAM corresponds to an intensification of westerlies in the high-latitude region and an anomalous southeasterly winds in the eastern subtropics [Hall and Visbeck, 2002]. The southeasterly anomalies decay toward the lower latitudes, inducing an anomalous Ekman upwelling in the eastern subtropics, which slackens the southward tilt of the isotherms and thus reducing the eastward flowing SICC. This effect reduces the vertical velocity shear and baroclinic instability of the SICC-SEC current system, leading to a weak eddy activity in the southeast Indian Ocean. In the same time, a positive SAM also leads to an intensification of oceanic heat loss in the eastern subtropics because of an intensification of the southeasterly trades and a slight gain of heat in the midlatitudes (Figure 11b). This anomalous meridional differential heating should reduce the meridional temperature gradient and thus the vertical velocity shear. However, this meridional differential heating is most pronounced in the interior ocean, but not near the coast where the instability analysis is performed. Therefore, it is the dynamic forcing, mostly the meridional geostrophic forcing associated with the SAM that works to modulate the meridional temperature gradient

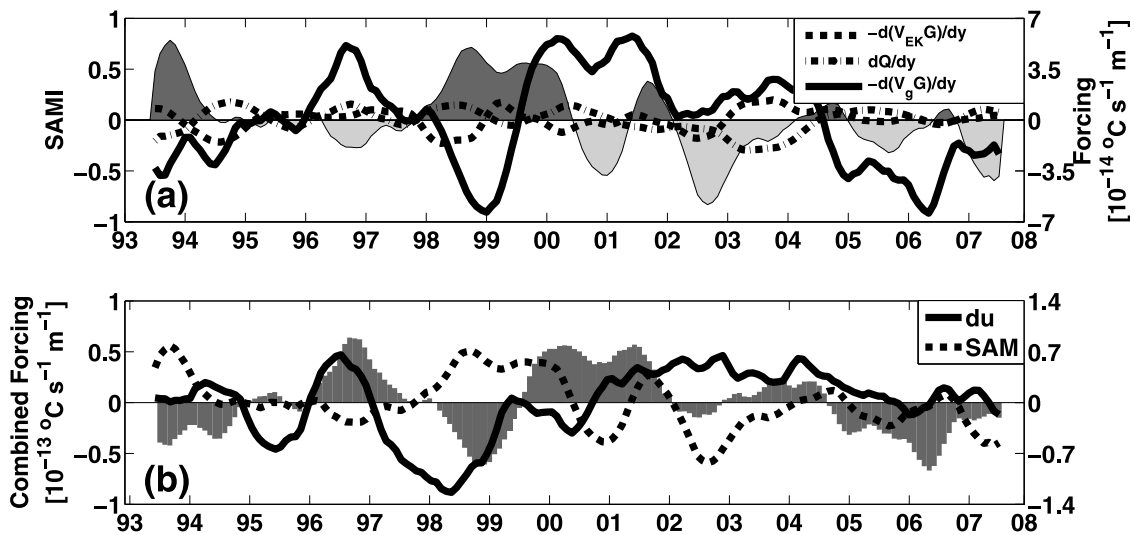


Figure 10. Time series of (a) meridional Ekman forcing term (dotted line), geostrophic forcing term (solid line), heat flux forcing term (dash-dotted line), and the SAM index (shaded areas) and (b) combined forcing (shaded bars), the vertical velocity shear (solid line), and the SAM index (dotted line). The forcing is averaged in (15°S–35°S, 100°E–110°E) over upper 150 m.

and thus the vertical velocity shear and the baroclinic instability of the SICC-SEC system.

6. Summary and Discussions

[26] In this paper, interannual modulation of mesoscale eddy activities in the southeast Indian Ocean along ~25°S is investigated on the basis of the 16 year satellite altimetry observations. It is found that the dynamic forcing associated with the SAM can modulate the baroclinic instability of the SICC-SEC current system, leading to changes of the EKE in the southeast Indian Ocean.

[27] Here, we emphasize the role of the SAM in the interannual modulation of the EKE in the southeast Indian Ocean, but do not exclude other impacts. Mesoscale eddy activities here can also be affected by other processes

because of a unique circulation system in this region, including the Leeuwin Current (LC). Studies have indicated that the LC variability also has a well-defined seasonal and interannual cycle [e.g., Feng et al., 2003; Morrow and Birol, 1998; Peter et al., 2005]. Feng et al. [2003] studied the ENSO related interannual variations of the Leeuwin Current at 32°S in this region and found the Leeuwin Current is stronger during a La Niña year and weaker during an El Niño year. Eddies and baroclinic Rossby waves are found to be generated by the LC variations and then propagate to the west [e.g., Rennie et al., 2007; Morrow et al., 2003; Birol and Morrow, 2001, 2003]. This appears to be supported by the correlation between the EKE in the southeast Indian Ocean and the Nino3.4 index, which shows a significant correlation when the Nino3.4 leads the EKE by

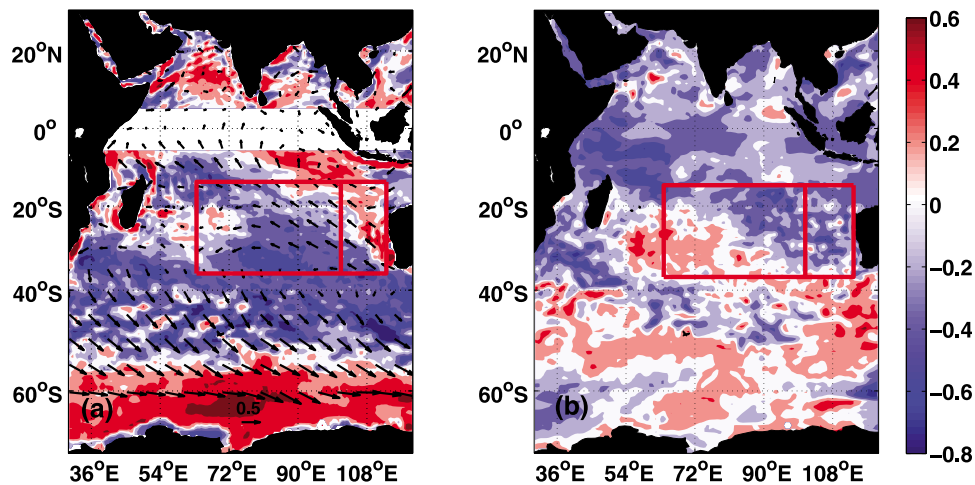


Figure 11. Synchronous correlation between the Southern Annular Mode index and (a) the wind stress (arrows) and Ekman pumping (shaded) and (b) net surface heat flux (positive downward). The data are low-pass filtered by applying a 1 year low-pass filter.

about 1 year (Figure 4b). Future studies are needed to quantify the effects of the eastern boundary processes in mesoscale processes in the interior ocean.

[28] **Acknowledgments.** This work is supported by China National Natural Science Foundation Projects (40788002, 40876001), China Foreign Expert “111” project through the Ministry of Education, and NSFC Creative Research Group Project (40921004). We are also very grateful to the two anonymous reviewers for their constructive comments.

References

- Birol, F., and R. Morrow (2001), Source of the baroclinic waves in the southeast Indian Ocean, *J. Geophys. Res.*, *106*, 9145–9160, doi:10.1029/2000JC900044.
- Birol, F., and R. Morrow (2003), Separation of the quasi-semiannual Rossby waves from the eastern boundary of the Indian Ocean, *J. Mar. Res.*, *61*, 707–723, doi:10.1357/002224003322981110.
- Carton, J. A., G. Chepurin, X. Cao, and B. Giese (2000), A simple ocean data assimilation analysis of the global upper ocean 1950–95. Part I: Methodology, *J. Phys. Oceanogr.*, *30*, 294–309, doi:10.1175/1520-0485(2000)030<0294:ASODAA>2.0.CO;2.
- Eden, C., and C. Böning (2002), Sources of eddy kinetic energy in the Labrador Sea, *J. Phys. Oceanogr.*, *32*, 3346–3363, doi:10.1175/1520-0485(2002)032<3346:SOEKEI>2.0.CO;2.
- Feng, M., G. Meyers, A. Pearce, and S. Wijffels (2003), Annual and interannual variations of the Leeuwin Current at 32°S, *J. Geophys. Res.*, *108*(C11), 3355, doi:10.1029/2002JC001763.
- Hall, A., and M. Visbeck (2002), Synchronous variability in the Southern Hemisphere atmosphere, sea ice, and ocean resulting from the annular mode, *J. Clim.*, *15*, 3043–3057, doi:10.1175/1520-0442(2002)015<3043:SVITSH>2.0.CO;2.
- Jia, F., L. Wu, and B. Qiu (2011), Seasonal modulation of eddy kinetic energy and its formation mechanism in the southeast Indian Ocean, *J. Phys. Oceanogr.*, in press.
- Ma, H., and L. Wu (2011), Global teleconnections in response to freshening over the Antarctic Ocean, *J. Clim.*, doi:10.1175/2010JCLI3634.1, in press.
- Marshall, G. J. (2003), Trends in the Southern Annular Mode from observations and reanalyses, *J. Clim.*, *16*, 4134–4143, doi:10.1175/1520-0442(2003)016<4134:TITSAM>2.0.CO;2.
- Marshall, G. J., A. Orr, N. P. M. van Lipzig, and J. C. King (2006), The impact of a changing Southern Hemisphere Annular Mode on Antarctic Peninsula summer temperatures, *J. Clim.*, *19*, 5388–5404, doi:10.1175/JCLI3844.1.
- Mo, K. C. (2000), Relationships between low-frequency variability in the Southern Hemisphere and sea surface temperature anomalies, *J. Clim.*, *13*, 3599–3610, doi:10.1175/1520-0442(2000)013<3599:RBLFVI>2.0.CO;2.
- Morrow, R., and F. Birol (1998), Variability in the southeast Indian Ocean from altimetry: Forcing mechanisms for the Leeuwin Current, *J. Geophys. Res.*, *103*, 18,529–18,544, doi:10.1029/98JC00783.
- Morrow, R., F. Fang, M. Feix, and R. Molcard (2003), Anatomy of three warm-core Leeuwin Current eddies, *Deep Sea Res.*, *50*, 2229–2243, doi:10.1016/S0967-0645(03)00054-7.
- Palastanga, V., P. J. van Leeuwen, M. W. Schouten, and W. P. M. de Ruijter (2007), Flow structure and variability in the subtropical Indian Ocean: Instability of the South Indian Ocean Countercurrent, *J. Geophys. Res.*, *112*, C01001, doi:10.1029/2005JC003395.
- Penduff, T., B. Barnier, W. K. Dewar, and J. J. O’Brien (2004), Dynamical response of the oceanic eddy field to the North Atlantic Oscillation: A model-data comparison, *J. Phys. Oceanogr.*, *34*, 2615–2629, doi:10.1175/JPO2618.1.
- Peter, B. N., P. Sreeraj, and K. G. Vimal Kumar (2005), Structure and variability of the Leeuwin Current in the south eastern Indian Ocean, *J. Indian Geophys. Union*, *9*(2), 107–119.
- Qiu, B. (1999), Seasonal eddy modulation of the North Pacific Subtropical Countercurrent: TOPEX/Poseidon observations and theory, *J. Phys. Oceanogr.*, *29*, 2471–2486, doi:10.1175/1520-0485(1999)029<2471:SEFMOT>2.0.CO;2.
- Qiu, B., and S. Chen (2004), Seasonal modulations in the eddy field of the South Pacific Ocean, *J. Phys. Oceanogr.*, *34*, 1515–1527, doi:10.1175/1520-0485(2004)034<1515:SMITEF>2.0.CO;2.
- Qiu, B., and S. Chen (2010a), Interannual variability of the North Pacific Subtropical Countercurrent and its associated mesoscale eddy field, *J. Phys. Oceanogr.*, *40*, 213–225, doi:10.1175/2009JPO4285.1.
- Qiu, B., and S. Chen (2010b), Eddy-mean flow interaction in the decadal modulating Kuroshio Extension system, *Deep Sea Res., Part II*, *57*, 1097–1110, doi:10.1016/j.dsr2.2008.11.036.
- Rao, S. A., and S. K. Behera (2005), Subsurface influence on SST in the tropical Indian ocean: Structure and interannual variability, *Dyn. Atmos. Oceans*, *39*, 103–135, doi:10.1016/j.dynatmoce.2004.10.014.
- Rayner, N. A., D. E. Parker, E. B. Horton, C. K. Folland, L. V. Alexander, D. P. Rowell, E. C. Kent, and A. Kaplan (2003), Global analyses of sea surface temperature, sea ice, and night marine air temperature since the late nineteenth century, *J. Geophys. Res.*, *108*(D14), 4407, doi:10.1029/2002JD002670.
- Rennie, S. J., C. B. Pattiaratchi, and R. D. McCauley (2007), Eddy formation through the interaction between the Leeuwin Current, Leeuwin Undercurrent and topography, *Deep Sea Res., Part II*, *54*, 818–836, doi:10.1016/j.dsr2.2007.02.005.
- Saji, N. H., B. N. Goswami, P. N. Vinayachandran, and T. Yamagata (1999), A dipole in the tropical Indian Ocean, *Nature*, *401*, 360–363, doi:10.1038/43854.
- Schott, F. A., S.-P. Xie, and J. P. McCreary Jr. (2009), Indian Ocean circulation and climate variability, *Rev. Geophys.*, *47*, RG1002, doi:10.1029/2007RG000245.
- Siedler, G., M. Rouault, and J. R. E. Lutjeharms (2006), Structure and origin of the subtropical South Indian Ocean Countercurrent, *Geophys. Res. Lett.*, *33*, L24609, doi:10.1029/2006GL027399.
- Silvestri, G., and C. Vera (2009), Nonstationary impacts of the Southern Annular Mode on Southern Hemisphere climate, *J. Clim.*, *22*, 6142–6148, doi:10.1175/2009JCLI3036.1.
- Thompson, D. W. J., and J. M. Wallace (2000), Annular modes in the extratropical circulation, part I: Month-to-month variability, *J. Clim.*, *13*, 1000–1016, doi:10.1175/1520-0442(2000)013<1000:AMITEC>2.0.CO;2.
- Webster, P. J., A. M. Moore, J. P. Loschnigg, and R. R. Leben (1999), Coupled oceanic-atmospheric dynamics in the Indian Ocean during 1997–98, *Nature*, *401*, 356–360, doi:10.1038/43848.
- Xie, S.-P., H. Annamali, and F. Schott (2002), Structure and mechanisms of south Indian Ocean climate variability, *J. Clim.*, *15*, 864–878, doi:10.1175/1520-0442(2002)015<0864:SAMOSI>2.0.CO;2.
- Yang, J., Q. Liu, S.-P. Xie, Z. Liu, and L. Wu (2007), Impact of the Indian Ocean SST basin mode on the Asian summer monsoon, *Geophys. Res. Lett.*, *34*, L02708, doi:10.1029/2006GL028571.

F. Jia, J. Lan, and L. Wu, Physical Oceanography Laboratory, Ocean University of China, 238 Songling Rd., Qingdao 266100, China. (afanayang31@163.com)

B. Qiu, Department of Oceanography, University of Hawai‘i at Mānoa, 100 Pope Rd., Honolulu, HI 96822, USA.